The Elastic Anisotropic and Thermodynamic Properties of $I4mm$-B_3C

Qingyang Fan[a], Qun Wei[b,*], Changchun Chai[a], Yintang Yang[a], Xinhai Yu[a], Yang Liu[a], Junping Zheng[a], Peikun Zhou[c] and Dongyun Zhang[d]

[a]State Key Discipline Laboratory of Wide BandGap Semiconductor Technology, School of Microelectronics, Xidian University, Xi'an 710071, PR China

[b]School of Physics and Optoelectronic Engineering, Xidian University, Xi'an 710071, PR China

[c] Faculty of Science, University of Paris-Sud, Paris 91400, France

[d]National Supercomputing Center in Shenzhen, Shenzhen 518055, PR China

(Received March 16, 2015)

The structural, elastic anisotropy and thermodynamic properties of the $I4mm$-B_3C are investigated using first-principles calculations and the quasi-harmonic Debye model. The calculated elastic anisotropic suggest that $I4mm$-B_3C is elastically anisotropic with its Poisson ratio, shear modulus, the Young modulus, the universal anisotropic index, shear anisotropic factors, and the percentage of elastic anisotropy for bulk modulus and shear modulus. The quasi-harmonic Debye model, using a set of total energy versus molar volume obtained with the first-principles calculations, is applied to the study of the thermal and vibrational effects. The thermal expansions, heat capacities, the Grüneisen parameters and the Debye temperatures dependence on the temperature and pressure are obtained in the whole pressure range from 0 to 90 GPa and temperature range from 0 to 2000 K.

DOI: 10.12693/APhysPolA.129.103

PACS: 71.15.Mb, 65.40.De, 62.20.de

1. Introduction

Diamond is well known for its mechanical, electrical, and chemical properties, including exceptional hardness, high hole and electron mobility, good thermal conductivity, wide band gap, and a large energy barrier. However, it cannot resist oxidation and reacts with ferrous metals, which largely limits its practical applications. All materials composed of boron and carbon appear to have better resistance to ferrous metals and oxygen than similar materials of C, since B has one less electron than C and is relatively easily incorporated into diamond due to its small atomic radius [1]. Therefore, one expects the diamond-like BC_x (d-BC_x) materials to combine the best properties of the elements such as high hardness, good electrical properties, and high chemical and thermal stability [2, 3]. Recently, d-BC_5 with superior capabilities has successfully been synthesized by a laser-heated diamond anvil cell at 24 GPa and approximately 2200 K [4]. The experimental characterizations of d-BC_5 indicate that it not only has large bulk modulus of 335 GPa, but also a high Vickers hardness of 71 GPa. The combination of these distinguished properties has stimulated many theoretical studies [5]. Nevertheless, the exact crystal structure has not been experimentally definitively determined due to the similar atomic numbers between B and C, which has led to different and even contradictory reports on d-BC_5 crystal structure and mechanical properties [6–9]. Liu et al. [10] have explored the crystal structures of synthesized diamond-like BC_3 (d-BC_3) with particle swarm optimization (PSO) algorithm, and found that the simulated Raman modes of $Pmma$ phase are in agreement with the experimental data. Recently, Mikhaylushkin et al. [11] predicted two stable boron carbides (BC_3 and BC_5) and found they are more stable than those previously reported. Li et al. [12] found that the hardness of the B–C system has a decreasing trend with the increase of boron concentration.

Recently, Wang et al. theoretically predicted that a new $I4mm$ phase for B_3C is mechanically and dynamically stable by means of applying PSO algorithm [13]. Our present work systematically investigates the elastic anisotropy of B_3C. In addition, the present work is also study of the pressure and temperature effects on the thermodynamic properties of B_3C using the first-principle calculations. The thermodynamic properties, such as heat capacity, thermal expansion, the Grüneisen parameters, and the Debye temperature are investigated by the quasi-harmonic Debye model.

2. Theoretical method

In this calculation, the structural optimization and property predictions of the $I4mm$-B_3C were performed using desity functional theory (DFT) [14, 15] with the generalized gradient approximation (GGA) parametrized by Perdew, Burke and Ernzerhof (PBE) [16] as implemented in the Cambridge Serial Total Energy Package

*corresponding author; e-mail: weiaqun@163.com

(CASTEP) code [17]. The total energy convergence tests showed that convergence to within 1 meV/atom was achieved with the above calculation parameters. In this calculation, a plane-wave basis set with energy cut-off 460 eV is used. The k-point samplings with $10\times10\times4$ in the Brillouin zone were performed using the Monkhorst–Pack scheme [18]. The Broyden–Fletcher–Goldfarb–Shanno (BFGS) [19] minimization scheme was used in geometry optimization. The self-consistent convergence of the total energy is 5×10^{-6} eV/atom; the maximum force on the atom is 0.01 eV/Å, the maximum ionic displacement within 5×10^{-4} Å and the maximum stress within 0.02 GPa.

In order to obtain the thermodynamic properties of $I4mm$-B_3C, the quasi-harmonic Debye model [20–23] is introduced, in which the non-equilibrium Gibbs function $G*(V:P,T)$ takes the form of $G*(x:P,T) = E(x)+PV(x)+A_{\rm vib}(\Theta(x):T)$. On the right-hand side of the equation, $E(x)$ is the total energy of the crystal, which corresponds to the potential energy surface as determined by most electronic structure or atomistic calculations. The second part, PV, corresponds to the constant hydrostatic pressure condition. Finally, the third part, $A_{\rm vib}$, is the vibrational Helmholtz free energy, which includes both the vibrational contribution to the internal energy and the $-TS$ constant temperature condition term. Then, before the quasi-harmonic Debye model can be properly applied, this multivariable surface has to be transformed into an $E(V)$ curve. The next step will consist in using the Debye model of the phonon density of states to write the vibrational Helmholtz free energy $A_{\rm vib}$, which can be followed by [24–28]:

$$A_{\rm vib}(\Theta;T) = nKT\Big[\frac{9}{8}\frac{\Theta}{T}+3\ln(1-{\rm e}^{-\Theta/T}) -D\left(\frac{\Theta}{T}\right)\Big]. \tag{1}$$

Here $D(\Theta/T)$ represents the Debye integral. Assume that y is equal to Θ/T, so

$$D(y) = \frac{3}{y^3}\int_0^y \frac{x^3}{{\rm e}^x-1}\,{\rm d}x, \tag{2}$$

n represents the number of atoms per formula unit, Θ represents the Debye temperature, expressed as [24]:

$$\Theta = \frac{h}{2\pi k}\left[6\pi^2V^{1/2}n\right]^{1/3} f(\nu)\sqrt{\frac{B_{\rm s}}{M}}, \tag{3}$$

where M represents the molecular mass per formula unit. B_s represents the adiabatic bulk modulus, the Poisson ratio v is taken as 0.23 in our calculation, and $f(v)$ is given by [26, 27]:

$$f(v) = \left\{3\left[2\left(\frac{2}{3}\frac{1+v}{1-2v}\right)^{3/2}+\left(\frac{1}{3}\frac{1+v}{1-v}\right)^{3/2}\right]^{-1}\right\}^{1/3}. \tag{4}$$

The isothermal bulk modulus and other thermal properties such as heat capacity at constant volume $C_{\rm v}$, the heat capacity at constant pressure $C_{\rm p}$, and thermal expansion α are respectively taken as [29]:

$$B_T = -x^{-2}B_0\,{\rm e}^{a(1-x)}f(x), \tag{5}$$

$$x = \left(\frac{V}{V_0}\right)^{1/3}, \tag{6}$$

$$f(x) = x-2-ax(1-x), \tag{7}$$

where $V_0 = V(0,T)$ is the zero-pressure equilibrium volume, B_0 is the zero-pressure bulk modulus, and a is given through the relation

$$a = 3(B_0'-1)/2, \tag{8}$$

where B_0' is first pressure derivative. In addition, B_0, B_0' and a are the fitting parameters and

$$C_V = 3nk\left[4D\left(\frac{\Theta}{T}\right)-\frac{3\Theta/T}{{\rm e}^{\Theta/T}-1}\right], \tag{9}$$

$$C_P = C_V(1+\alpha\gamma T), \tag{10}$$

$$\alpha = \frac{\gamma C_V}{B_T V}, \tag{11}$$

where C_V is the heat capacity and γ represents the Grüneisen parameter and it is expressed as

$$\gamma = -\frac{{\rm d}\ln\Theta(V)}{{\rm d}\ln V}. \tag{12}$$

3. Results and discussion

3.1. Elastic properties and anisotropic properties

B_3C has a tetragonal symmetry that belongs to the $I4mm$ space group. The calculated equilibrium lattice parameters $a = 2.832$, $c = 7.081$ within GGA method for $I4mm$-B_3C are reasonably compared with previous study [13]. For $I4mm$-B_3C, there is no available experimental result. However, our calculated lattice parameters using GGA agree well with the previously reported value of Wang et al. [13], calculated using the projector augmented wave (PAW) method. The elastic properties (including elastic constants, elastic modulus, etc.) give important information concerning the nature of the forces operating in solids. In this paper, we calculated the elastic constants and elastic modulus of $I4mm$-B_3C. For the tetrahedral $I4mm$-B_3C, there are six independent elastic constants C_{ij} (C_{11}, C_{12}, C_{13}, C_{33}, C_{44} and C_{66}), C_{11} = 525 GPa, C_{12} = 11 GPa, C_{13} =120 GPa, C_{33} = 701 GPa, C_{44} = 201 GPa, and C_{66} = 54 GPa. The calculated constants elastic modulus, such as bulk modulus B = 244 GPa, shear modulus G = 182 GPa, the Young modulus E = 437 GPa and the Poisson ratio ν =0.201 of B_3C are reasonably compared with previous study [13]. The Young modulus (E) and the Poisson ratio (ν) are major elastic parameters of materials calculated using the formula $E = 9BG/(3B+G)$ and $v = (3B-2G)/[2(3B+G)]$, respectively.

It is well known that the anisotropy of elasticity is an important implication in engineering science and crystal physics. The directional dependence of anisotropy was calculated using the program Elastics Anisotropy Measures (ELAM) [30]. The stiffness tensor expresses the stress tensor in terms of the strain tensor: $\sigma_{ij} = C_{ijkl}\varepsilon_{kl}$.

C_{ijkl} is elastic stiffness constant. The compliance tensor is the inverse of the stiffness tensor and interprets the strain tensor in terms of the stress tensor: $\varepsilon_{ij} = S_{ijkl}\sigma_{kl}$. The S_{ijkl} is the elastic compliance constant. The Young modulus is defined as the ratio of normal stress to linear normal strain (both in the direction of applied load). The shear modulus is defined as the ratio of shear stress to linear shear strain. The Poisson ratio is defined as the ratio of transverse strain (normal to the applied load) to axial strain (in the direction of the applied load).

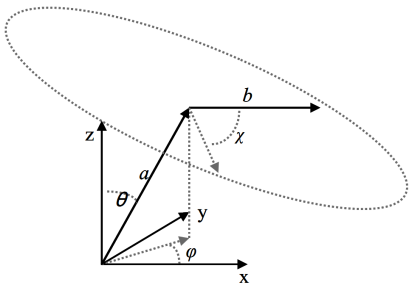

Fig. 1. Definitions of angles used to describe directions in calculations.

A fourth order tensor transforms in a new basis set following the rule:

$$S'_{\alpha\beta\gamma\delta} = r_{\alpha i} r_{\beta j} r_{\gamma k} r_{\delta l} S_{ijkl}, \tag{13}$$

where the Einstein summation rule is adopted and where the $r_{\rho m}$ is the component of the rotation matrix (or direction cosines). The transformation can be substantially simplified in calculation of specific modulus. The uniaxial stress can be represented as a unit vector, and advantageously described by two angles (θ, φ), we choose it to be the first unit vector in the new basis set a. The determination of some elastic properties (shear modulus, the Poisson ratio) requires another unit vector b, perpendicular to unit vector a, and characterized by the angle χ. It is fully characterized by the angles θ $(0, \pi)$, φ $(0, 2\pi)$ and χ $(0, 2\pi)$, as illustrated in Fig. 1. The coordinates of two vectors are

$$a = \begin{pmatrix} \sin\theta\cos\phi \\ \sin\theta\sin\phi \\ \cos\theta \end{pmatrix},$$

and

$$b = \begin{pmatrix} \cos\theta\cos\phi\cos\chi - \sin\phi\sin\chi \\ \cos\theta\sin\phi\cos\chi + \cos\phi\sin\chi \\ -\sin\theta\cos\chi \end{pmatrix}. \tag{14}$$

The Young modulus can be obtained by using a purely normal stress in $\varepsilon_{ij} = S_{ijkl}\sigma_{kl}$ in its vectors form and it is given by

$$E(\theta,\phi) = \frac{1}{S'_{1111}} = \frac{1}{r_{1i}r_{1j}r_{1k}r_{1l}S_{ijkl}} = \frac{1}{a_i a_j a_k a_l S_{ijkl}}. \tag{15}$$

Other properties depending on two directions (if perpendicular this corresponds to 3 angles) make them difficult to represent graphically. A convenient possibility is then to consider three representations: minimum, average and maximum. For each θ and φ, the angle χ is scanned and the minimum, average and maximum values are recorded for this direction. The shear modulus is obtained by applying a pure shear stress in the vector form and results in

$$G(\theta,\phi,\chi) = \frac{1}{4S'_{1212}} = \frac{1}{4r_{1i}r_{2j}r_{1k}r_{2l}S_{ijkl}} = \frac{1}{4a_i a_j a_k a_l S_{ijkl}}. \tag{16}$$

The Poisson ratio can be expressed as

$$\nu(\theta,\phi,\chi) = \frac{S'_{1122}(\theta,\phi,\chi)}{S'_{1111}(\theta,\phi,\chi)} = \frac{r_{1i}r_{1j}r_{2k}r_{2l}S_{ijkl}}{r_{1i}r_{1j}r_{1k}r_{1l}S_{ijkl}} = -\frac{a_i a_j b_k b_l S_{ijkl}}{a_i a_j a_k a_l S_{ijkl}}. \tag{17}$$

Using the above anisotropic formulae, the calculated values of the Poisson ratio, shear modulus and the Young modulus along different directions as well as the projections in different planes were shown in Fig. 2 and Fig. 3. The black line represents maximum and red line represents minimum. We first focus on the Poisson ratio, Fig. 2a,b, and c display the 2D representation of the Poisson ratio in the xy, xz, and yz planes for $I4mm$-B_3C, respectively. We found that $0 \leq v \leq 0.70$, showing that v remains positive (no negative Poisson ratio) at 0 GPa.

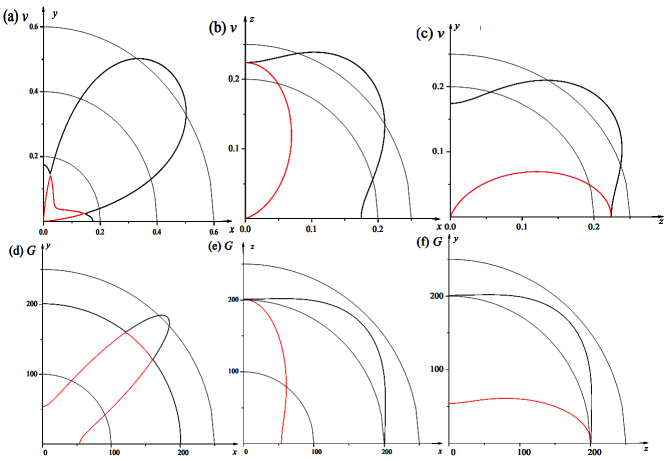

Fig. 2. 2D representation of the Poisson ratio for $I4mm$-B_3C in the xy plane (a), xz plane (b), and yz plane (c) and for $I4mm$-B_3C in the xy plane (d), xz plane (e), and yz plane (f).

In order to quantify the anisotropy, we calculated the shear modulus for all possible directions of shear strain, the 2D representation of shear modulus in the xy, xz, and yz planes for $I4mm$-B_3C are shown in Fig. 2 d,e, and f, respectively. The black line represents maximum and red line represents minimum. We observed that shear modulus varies between 54 and 257 GPa, the

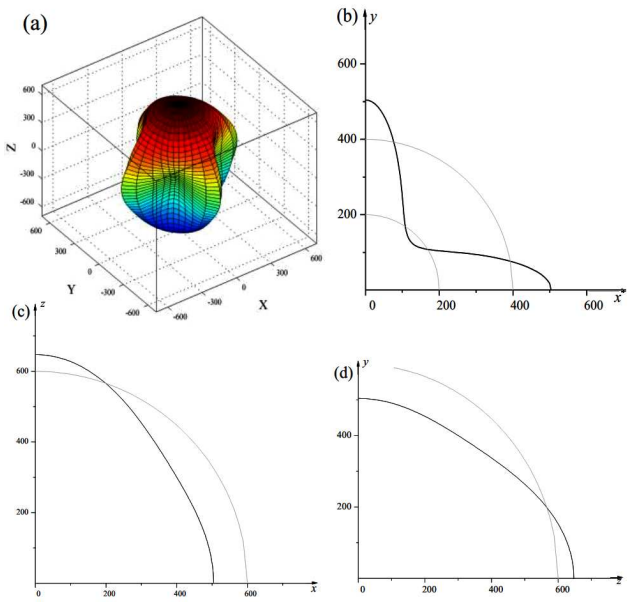

Fig. 3. The directional dependence of the Young modulus for $I4mm$-B_3C (a), 2D representation of the Poisson ratio in the xy plane (b), xz plane (c), and yz plane (d).

ratio $G_{\max}/G_{\min}$ =4.76, the average value of all directions is 169 GPa, this value is very close to castep value (164 GPa). At last, we focus on the Young modulus, which is plotted as the directional dependence of the Young modulus at different pressure, the xy, xz, and yz planes for $I4mm$-B_3C in Fig. 3a-d, respectively. It is clearly visible that the Young modulus for this material is large anisotropic, with a minimal value of $E_{\min}$ = 177 GPa and a maximum of $E_{\max}$ = 647 GPa, the average value of all directions is 448 GPa, this value is very close to castep value (437 GPa, $E = 9BG/(3B+G)$ [31]), the ratio $E_{\max}/E_{\min}$ = 3.66. Therefore, $I4mm$-B_3C exhibits a large anisotropy in its Poisson ratio, shear modulus and the Young modulus.

It is well known that microcracks are induced in ceramics owing to the anisotropy of the coefficient of thermal expansion as well as elastic anisotropy. Hence it is important to calculate elastic anisotropy in structural compounds in order to understand these properties. The shear anisotropic factors provide a measure of the degree of anisotropy in the bonding between atoms in different planes. The shear anisotropic factor for the {100} shear planes between the ⟨011⟩ and ⟨010⟩ directions is [32]:

$$A_1 = \frac{4C_{44}}{C_{11} + C_{33} - 2C_{13}}. \tag{18}$$

For the {001} shear plane between ⟨110⟩ and ⟨010⟩ directions it is [32]:

$$A_2 = \frac{2C_{66}}{C_{11} - C_{12}}. \tag{19}$$

For an isotropic crystal the factors A_1 and A_2 must be one, while any value smaller or greater than unity is a measure of the degree of elastic anisotropy possessed by the crystal. The calculated value of A_1 and A_2 is 0.82 and 0.21 at ambient pressure, respectively. The elastic anisotropy of a crystal can be characterized by many different ways. Therefore we calculate several anisotropic indices, such as the universal anisotropic index (A^U) [33] and the percentage of elastic anisotropy for bulk modulus (A_B) and shear modulus (A_G) [34] in this paper. The equations used are shown in the following:

$$A^U = 5\frac{G_V}{G_R} + \frac{B_V}{B_G} - 6 \geq 0, \tag{20}$$

$$A_B = \frac{B_V - B_R}{B_V + B_R}, \tag{21}$$

$$A_G = \frac{G_V - G_R}{G_V - G_R}. \tag{22}$$

It is clear that for an isotropic structure, all indices in Eqs. (20)–(22) are zero. The large deviations from zero indicate the high anisotropic mechanical properties. The A^U, A_B and A_G values are 1.302, 0.024, and 0.111 for $I4mm$-B_3C, respectively. From all calculated anisotropic parameters, it is easily concluded that the $I4mm$-B_3C compounds show elastic anisotropy.

3.2. Thermodynamic properties

The thermal expansion α with pressures and temperatures for $I4mm$-B_3C are shown in Fig. 4. From Fig. 4, as the pressure increases, the thermal expansion coefficient αdecreases, and the higher the temperature is, the faster the thermal expansion coefficient α reduces. As pressure increases, α decreases rapidly at high temperature and the effects of temperature become less and less pronounced. This is an indication of the inadequacy of the quasi-harmonic approximation at elevated temperatures and pressures. From Fig. 4, we can find that the effect of temperature on the thermal expansion is not as significant as that of pressure in our calculated pressure and temperature ranges.

The calculated relationships of the Debye temperature Θ_D on pressure and temperature are plotted in Fig. 5a. The Θ_D is affected by both pressure and temperature, and the affect of increasing pressure on $I4mm$-B_3C is the same as decreasing temperature. One can find: when the applied pressure changes from 0 GPa to 90 GPa, the Debye temperature increases by 41.14%, 42.24%, 46.08%, 51,66%, 59.20% and 68.83% at temperatures of 0, 400, 800, 1200, 1600, and 2000 K, respectively. At a given temperature, the Θ_D increases quickly with increasing pressure. In a word, we can see that the Debye temperature decreases with the temperature at certain pressure and increases with the pressure at certain temperature. From Fig. 5a, the effect of the temperature on the Debye temperature is less significant than that of pressure on it. The Grüneisen parameter, which describes the alteration in a crystal lattices vibration frequency, can reasonably predict the anharmonic properties of a solid, such as the temperature dependence of phonon frequencies and lattice volume. Usually, the Grüneisen parameter is posi-

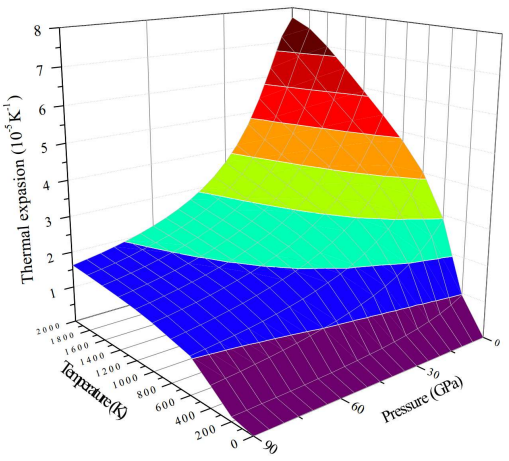

Fig. 4. Three-dimensional surface plots of thermal expansion versus pressure and temperature for *I*4*mm*-B_3C.

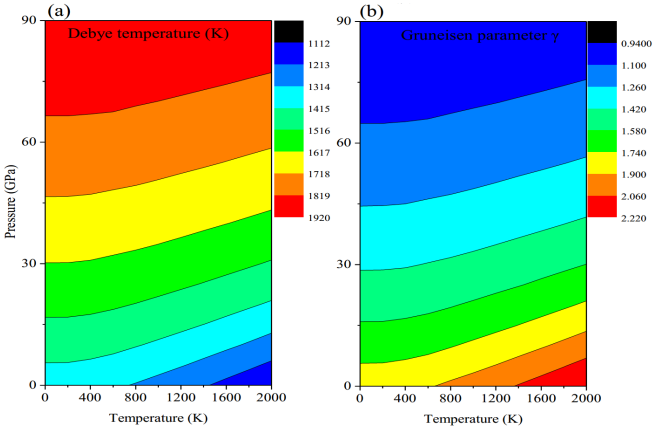

Fig. 5. Two-dimensional contour plots of Debye temperature (a), and Grüneisen parameter (b) versus pressure and temperature for $P4_2/$mnm-BC.

tive and lies in the range 1.5 ± 1.0. The calculated relationships of the Grüneisen parameter γ on pressure and temperature are plotted in Fig. 5b. It is found that the Grüneisen parameter slightly increases with temperature at a given pressure, but decreases with pressure at a given temperature. From Fig. 5b, we can find that the effect of the pressure on the Grüneisen parameter is more significant than that of temperature on it.

Figure 6 shows the two-dimensional contour plots of the dependence of the heat capacity on pressure and temperature. The heat capacity of the Debye model, which only contains these low frequency modes excited at low temperature, is an important measure for thermodynamic properties. The difference between C_P and C_V is very small at low temperatures and low pressures. At high temperature, the calculated heat capacity is expected to converge to a constant $3N_Ak_B \approx 99.69$ J mol^{-1} K^{-1} according to the law of Dulong and

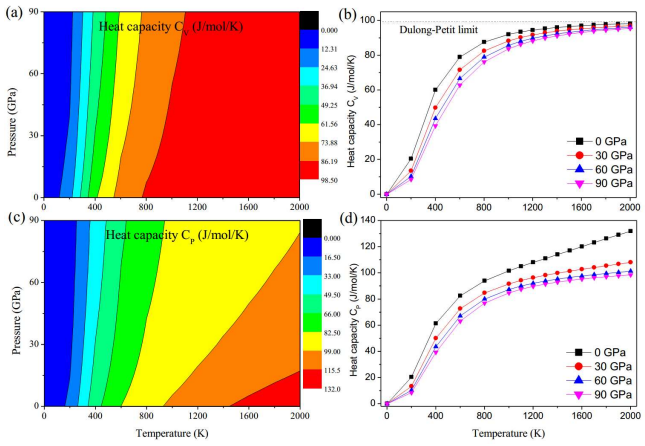

Fig. 6. Calculated specific pressure heat capacity C_P and volume heat capacity C_V as a function of pressure for *I*4*mm*-B_3C at different temperature: C_V contours (a), $C_V - T$ contours (b), C_P contours (c), and $C_P - T$ contours (d).

Petit. From Fig. 6, one can also see that the heat capacity (C_P and C_V) increases with the temperature at the same pressure and decreases with the pressure at the same temperature. The influences of the temperature on the heat capacity are much more significant than that of the pressure. It also shows that when $T < 800$ K, the heat capacity are sensitive to both temperature and pressure.

4. Conclusion

The structural properties, elastic properties, elastic anisotropy, and thermodynamic properties of the newly predicted *I*4*mm*-B_3C are investigated and analyzed by the first-principles calculations in combination with the quasi-harmonic Debye model. The calculated lattice parameters, elastic constants, and elastic modulus are in good agreement with the previous data. The *I*4*mm*-B_3C exhibits a large anisotropy in its Poisson ratio, shear modulus, the Young modulus, shear anisotropic factors, A^U, A_B, and A_G. Moreover, the thermal expansions, heat capacities, the Grüneisen parameters and the Debye temperatures dependence on the temperature and pressure are obtained in the whole pressure range from 0 to 90 GPa and temperature range from 0 to 2000 K.

Acknowledgments

This work was financially supported by the Fundamental Research Funds for the Central Universities, Natural Science Foundation of China (No. 11204007), and Natural Science Basic Research plan in Shaanxi Province of China (grant No. 2013JQ1007).

References

[1] E.A. Ekimov, V.A. Sidorov, E.D. Bauer, N.N. Melnik, N.J. Curro, J.D. Thompson, S.M. Stishov, *Nature* **428**, 542 (2004).

[2] L.E. Jones, P.A. Thrower, *Carbon* **29**, 251 (1991).

[3] J. Isberg, J. Hammersberg, E. Johansson, T. Wikström, D.J. Twitchen, A.J. Whitehead, S.E. Coe, G.A. Scarsbrook, *Science* **297**, 1670 (2002).

[4] V.L. Solozhenko, O.O. Kurakevych, D. Andrault, Y.L. Godec, M. Mezouar, *Phys. Rev. Lett.* **102**, 015506-4 (2009).

[5] P. Lazar, R. Podloucky, *Appl. Phys. Lett.* **94**, 251904 (2009).

[6] M. Calandra, F. Mauri, *Phys. Rev. Lett.* **101**, 016401 (2008).

[7] Y. Yao, J.S. Tse, D.D. Klug, *Phys. Rev. B* **80**, 094106 (2009).

[8] R.F. Zhang, S. Veprek, A.S. Argon, *Phys. Rev. B* **80**, 233401 (2009).

[9] S.M. Nkambule, J.E. Lowther, *Solid State Commun.* **150**, 133 (2010).

[10] H.Y. Liu, Q. Li, L. Zhu, Y.M. Ma, *Phys. Lett. A* **375**, 771 (2011).

[11] A.S. Mikhaylushkin, X. Zhang, A. Zunger, *Phys. Rev. B* **87**, 094103 (2013).

[12] M.M. Li, X. Fan, W.T. Zheng, *J. Phys. Condens. Matter* **25**, 425502 (2013).

[13] D.Y. Wang, Q. Yan, B. Wang, Y.X. Wang, J.M. Yang, G. Yang, *J. Chem. Phys.* **140**, 224704 (2014).

[14] P. Hohenberg, W. Kohn, *Phys. Rev.* **136**, B864 (1964).

[15] W. Kohn, L.J. Sham, *Phys. Rev.* **140**, A1133 (1965).

[16] J.P. Perdew, K. Burke, M. Ernzerhof, *Phys. Rev. Lett.* **77**, 3865 (1996).

[17] S.J. Clark, M.D. Segall, C.J. Pickard, P.J. Hasnip, M.I.J. Probert, K. Refson, M.C. Payne, *Z. Kristallogr.* **220**, 567 (2005).

[18] H.J. Monkhorst, J.D. Pack, *Phys. Rev. B* **13**, 5188 (1976).

[19] B.G. Pfrommer, M. Cote, S.G. Louie, M.L. Cohen, *J. Comput. Phys.* **131**, 233 (1997).

[20] M.A. Blanco, E. Francisco, V. Luaña, *Comput. Phys. Commun.* **158**, 57 (2004).

[21] F. Peng, H.Z. Fu, X.L. Cheng, *Physica B* **400**, 83 (2007).

[22] F. Peng, H.Z. Fu, X.D. Yang, *Solid State Commun.* **145**, 91 (2008).

[23] F. Peng, H.Z. Fu, X.D. Yang, *Physica B* **403**, 2851 (2008).

[24] M.A. Blanco, Ph.D. Thesis, Universidad de Oviedo, 1997.

[25] M.A. Blanco, A. Martín Pendás, E. Francisco, J.M. Recio, R. Franco, *J. Molec. Struct. Theochem.* **368**, 245 (1996).

[26] E. Francisco, J.M. Recio, M.A. Blanco, A. Martín Pendás, *J. Phys. Chem. A* **102**, 1595 (1998).

[27] E. Francisco, G. Sanjurjo, M.A. Blanco, *Phys. Rev. B* **63**, 094107 (2001).

[28] M. Flórez, J.M. Recio, E. Francisco, M.A. Blanco, A. Martín Pendás, *Phys. Rev. B* **66**, 144112 (2002).

[29] P. Vinet, J.H. Rose, J. Ferrante, J.R. Smith, *J. Phys. Condens. Matter.* **1**, 1941 (1989).

[30] A. Marmier, Z.A.D. Lethbridge, R.I. Walton, C.W. Smith, S.C. Parker, K.E. Evans, *Comput. Phys. Commun.* **181**, 2102 (2010).

[31] R. Hill, *Proc. Phys. Soc. Lond.* **65**, 349 (1952).

[32] D. Connétable, O. Thomas, *Phys. Rev. B* **79**, 094101 (2009).

[33] I.R. Shivakumar, M. Ostoja-Starzewski, *Phys. Rev. Lett.* **101**, 055504 (2008).

[34] D.H. Chung, W.R. Buessem, *Anisotropy in Single Crystal Refractory Compound*, 2nd ed., p. 217, Springer Science+Business Media, New York 1968.